



UNIVERSITY OF LEEDS

This is a repository copy of *Deterministic normal contact of rough surfaces with adhesion using a surface integral method*.

White Rose Research Online URL for this paper:
<http://eprints.whiterose.ac.uk/166540/>

Version: Accepted Version

Article:

Ghanbarzadeh, A orcid.org/0000-0001-5058-4540, Faraji, M and Neville, A (2020) Deterministic normal contact of rough surfaces with adhesion using a surface integral method. *Proceedings of the Royal Society A: Mathematical, Physical and Engineering Sciences*, 476 (2242). p. 20200281. ISSN 1364-5021

<https://doi.org/10.1098/rspa.2020.0281>

© 2020 The Author(s). Published by the Royal Society. All rights reserved. This is an author produced version of an article published in *Proceedings of the Royal Society A: Mathematical, Physical and Engineering Sciences*. Uploaded in accordance with the publisher's self-archiving policy.

Reuse

Items deposited in White Rose Research Online are protected by copyright, with all rights reserved unless indicated otherwise. They may be downloaded and/or printed for private study, or other acts as permitted by national copyright laws. The publisher or other rights holders may allow further reproduction and re-use of the full text version. This is indicated by the licence information on the White Rose Research Online record for the item.

Takedown

If you consider content in White Rose Research Online to be in breach of UK law, please notify us by emailing eprints@whiterose.ac.uk including the URL of the record and the reason for the withdrawal request.



eprints@whiterose.ac.uk
<https://eprints.whiterose.ac.uk/>

31 between them (1). Often in engineering, in particular solid mechanics, adhesion is referred to
32 as the attractive forces between non-bonding atoms or molecules of surfaces and the Lennard-
33 Jones is often used as a model potential providing a qualitative description of intermolecular
34 forces to describe the attraction/repulsion as a function of their separation. When two real
35 engineering bodies come into contact, there will be areas of surfaces which are in physical
36 contact and the contact pressure is compressive. Depending on the topography of the surfaces,
37 there will be a distribution of surface separations across the nominal contact area. These
38 separations, if small enough (with respect to atomic distances), can lead to attractive forces
39 between surface points.

40 In contact mechanics, there are numerous models of adhesive contact (2). In particular, there
41 are two widely-used analytical adhesive models both developed for smooth surfaces; namely
42 Johnson-Kendall-Roberts (JKR) (3) and Derjaguin-Muller-Toporov (DMT) (4). In JKR, it is
43 assumed that there is no adhesion outside the contact area and infinitely large pressures are
44 present at the border and inside the contact area. In contrast, DMT assumes a Hertzian contact
45 area with consideration of adhesion and adhesion forces do not contribute to surface
46 deformations. Both models have their limitations in application which makes JKR valid for the
47 case of soft materials and large radius of curvature and DMT valid for stiffer materials with
48 small curvatures. There is a wealth of engineering problems that would sit outside these
49 constraints and also a high proportion of engineering contact problems involve rough surfaces.
50 David Tabor showed that the validity of the JKR and DMT models can be assessed by the
51 Tabor parameter (μ) (5) where JKR can effectively predict adhesion at large values of (μ) and
52 DMT at smaller values. Maugis (6) developed a model based on the Dugdale approximation
53 using Lennard-Jones potentials and bridged the transition gap between DMT and JKR which,
54 to-date, stays a more complete description of the adhesive contact model for smooth surfaces.
55 Muller et al. (7) and later Greenwood (8) have developed a complete numerical solution for the
56 contact with adhesion by applying Lennard-Jones potential and elastic deformation of solid
57 surfaces. Greenwood has shown that the load-displacement curve becomes S-shaped at Tabor
58 values of more than one.

59 A great challenge in modelling contact of engineering surfaces with adhesion, is the irregular
60 nature of the surface topography which makes the application of analytical models almost
61 impossible. The pioneering work of Fuller et al. (9) shed light on the effect of roughness on
62 adhesion by development of an asperity-based adhesion model. Other significant contributions

63 in the field were reported by Persson (10) who used the self-affine fractal properties of the
64 surfaces and showed the dependency of adhesion on the fractal dimensions.

65 All the above-mentioned theoretical works have led to significantly increased understanding
66 of the nature of adhesive forces on the contact of surfaces. However, they lack deterministic
67 capabilities to account for the interactions of real surface topographies. In recent years, an
68 increase in computational power has resulted in the development of advanced numerical
69 models that can calculate adhesive contact of deterministic surface topographies. In a recent
70 contact mechanics challenge, Müser et al. (11) presented and compared the results of different
71 numerical approaches for calculation of the adhesive contact of a pre-defined experimentally
72 measured surface roughness. They have shown that numerical approaches such as Boundary
73 Element Method (BEM) (12), all-atom Molecular Dynamics (MD) (13) and Boundary Value
74 Methods (BVM) (14) can successfully calculate the contact problem with adhesion. In recent
75 years, there has been numerous works considering the contact of rough surfaces with adhesion.
76 Rey et al. (15) developed a BEM based contact mechanics model based on Fast Fourier
77 Transforms by minimising the potential energy that is the sum of elastic energy and adhesive
78 energy. Solhjo and Vakis (13) have developed an MD model using the Embedded Atom
79 Method (EAM) that simulates surface roughness with atoms and gives a high accuracy in
80 contact area calculations and surface pressure, though time-consuming and limited with the
81 number of atoms considered for simulations. Pastewka and Robbins (16) developed a Green's
82 function MD simulation to calculate non-adhesive contact of rough surfaces and proposed a
83 criterion for macroscopic adhesion based on the geometry and material properties.

84 Other significant contributions were made by Ciavarella in a series of articles (2, 17, 18). They
85 correlated Bearing Area Model (BAM) and geometrical intersections to adhesion via a simple
86 mathematical description (19). The model was reported to be valid for an intermediate range
87 of Tabor parameters. Pohrt and Popov (20-22) developed a BEM contact mechanics model that
88 utilised a mesh-dependant detachment criteria for adhesive contact of rough surfaces which
89 was based on the solution of non-adhesive contacts. Ghanbarzadeh et al. (23) used the same
90 model and predicted the bouncing behaviour of elasto-plastic and adhesive solids and showed
91 the significance of the effect of roughness in increasing the energy dissipation. Bazrafshan et
92 al. (24) developed a BEM based contact mechanics model and incorporated adhesive
93 interactions by means of Dugdale approximation and later studied the effect of roughness and
94 adhesion on the stick/slip of dissimilar materials (25). Medina and Dini (12) developed a
95 deterministic adhesive contact model using Multi-Level-Multi-Integration (MLMI) and

96 implemented adhesion by directly using Lennard-Jones potentials and integrating that over the
97 length of computational nodes to better represent adhesive pressures and to avoid convergence
98 issues due to the non-linear behaviour of the Lennard-Jones potential.

99 As discussed, the literature contains extensive and continuously evolving research in
100 mechanics of contacts in the presence of surface roughness and adhesion. Computational
101 models are becoming increasingly more efficient such that it is now possible using a desktop
102 PC to solve a contact problem in a reasonable time. This paper, represents an advancement in
103 the fully-deterministic calculation of normal contact of rough surfaces with adhesion by
104 directly using Lennard-Jones potential fields and integration methods over a surface area
105 around the computational nodes to offer an efficient and highly accurate computational model
106 for contact mechanics with adhesion. The model is an advancement to the line integral model
107 developed by Medina and Dini (12) that considered the integration in one dimension. The main
108 aim of the paper is to present this new mathematical model and to show the capabilities of the
109 model by comparing the results with already existing literature. The validity of the model is
110 tested for the case of smooth surfaces and results are compared with the results of Greenwood
111 (8). The strength of the model to capture the rough surface adhesive contact is also tested by
112 reproducing the results of the contact mechanics challenge reported by Müser et al. (11). Also
113 the idea that RMS slope of surface roughness is important in determining the adhesion force
114 has been highlighted by the model and a recent theory proposed by Li et al. (22) based a
115 modified Johnson parameter has been tested. The method presented here can be also applied to
116 cases where surface geometries are given by analytic functions such as the case of parabolic or
117 spherical geometries by only integrating the height functions with respect to X and Y lateral
118 dimensions. The theory of the model is presented in Section 2 followed by results and
119 discussion in Section 3.

120 **2 Theory**

121 **2.1 Non-adhesive normal contact**

122 The model uses a contact mechanics solver developed previously for non-adhesive contact of
123 rough surfaces using a BEM approach and incorporating Fast Fourier Transform (FFT) for
124 numerical efficiency. When two engineering surfaces with roughness come into contact, due
125 to the inhomogenous nature of the surface roughness, a small proportion of the nominal contact
126 area will sustain the load, known as the real area of contact.

127 The composite deformation of the surfaces $u_e(X, Y)$ due to the applied load of $p(X, Y)$ can be
 128 calculated by the linear convolution according to Boussinesq-Cerruti theory:

$$129 \quad u_e = K * p_d = \int_{-\infty}^{+\infty} \int_{-\infty}^{+\infty} K(X - \xi, Y - \eta) p(\xi, \eta) d\xi d\eta \quad (1)$$

130 in which x and y are two-dimensional coordinates, K is the convolution kernel and can be
 131 calculated from the half-space approximation as the following:

$$132 \quad K(X - \xi, Y - \eta) = \frac{1}{\pi E^*} \frac{1}{\sqrt{(X - \xi)^2 + (Y - \eta)^2}} \quad (2)$$

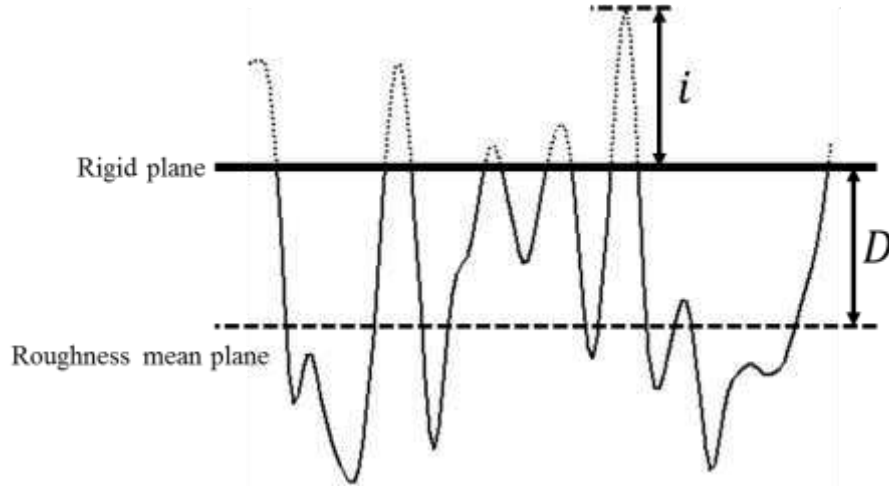
133 where E^* is the composite elastic modulus of both materials ($\frac{1}{E^*} = \frac{(1-\nu_1^2)}{E_1} + \frac{(1-\nu_2^2)}{E_2}$).
 134 Here, ν_1, ν_2, E_1 and E_2 are the Poisson's ratio and Elastic Moduli of materials 1 and 2
 135 respectively. For the contact of two rough surfaces, one can consider the composite roughness
 136 of the two contacting surfaces and a rigid plane to calculate the contacting points (26). By
 137 movement of the rigid body in the normal direction, the interference (i) between the contacting
 138 surfaces can be obtained (see Figure 1). For the nodes experiencing contact, the elastic
 139 deformation must be equal to the body interference and the pressure is generated at the asperity.
 140 The summation of the pressures on the nodes must also be equal to the applied load. Therefore,
 141 the set of equations for the contact of rough surfaces is as follows:

$$u_e(X, Y) = i(X, Y) = H(X, Y) - D(X, Y) \quad \forall (X, Y) \in A_e \quad (3.1)$$

$$p(X, Y) > 0 \quad \forall (X, Y) \in A_e \quad (3.2)$$

$$W = \iint p(X, Y) dXdY \quad (3.3)$$

142 where i is the asperity interference, H is the composite surface roughness height, D is the
 143 distance between reference plane and the rigid plane and W is the total applied load. The
 144 separation of asperities can be defined by $g(X, Y) = D(X, Y) - H(X, Y) + u(X, Y)$.



145

146

Figure 1 Schematic of the contact of rough surfaces

147

2.2 Adhesion model

148

In this paper, adhesive pressures are calculated at the areas of asperity separation by means of direct implementation of Lennard-Jones potential. The potential was first defined by John Lennard-Jones in the following format:

149

150

151

$$v = 4\epsilon \left[\left(\frac{\sigma}{r} \right)^{12} - \left(\frac{\sigma}{r} \right)^6 \right] \quad (4)$$

152

Where v is the interatomic potential, ϵ is the depth of the potential well, σ is the distance between particles at which the potential becomes zero and r is the finite separation of the two particles. Differentiation of Equation 4 with respect to r (separation) results in the determination of the force applied on the particles. Similarly, if potential energy per unit area is differentiated with respect to r , an expression for pressure is determined as in the following:

153

154

155

156

157

$$p(z) = \frac{8w_0}{3z_0} \left\{ \left(\frac{z_0}{z} \right)^9 - \left(\frac{z_0}{z} \right)^3 \right\} \quad (5)$$

158

where w_0 is the work of adhesion and can be measured experimentally or is calculated by integration of pressure with respect to separation from $z = z_0$ to $z = \infty$:

159

160

$$w_0 = \int_{z_0}^{\infty} p(z) dz \quad (6)$$

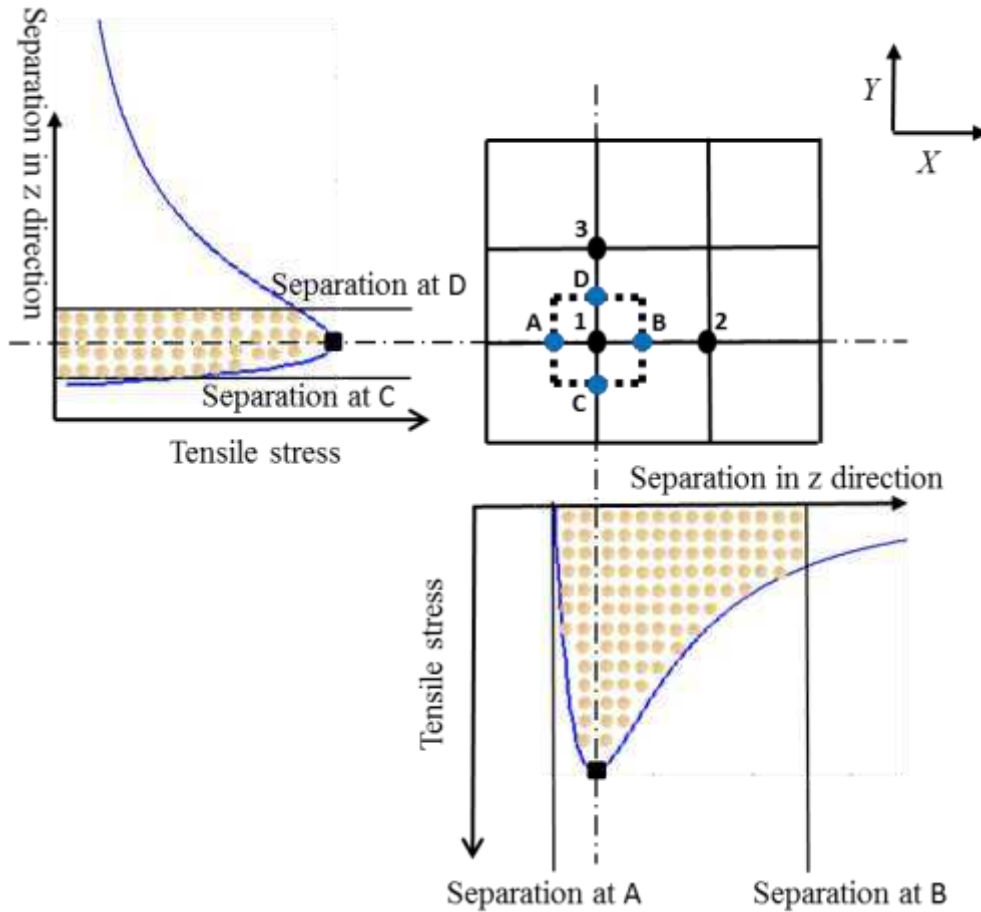
161

z_0 is the equilibrium separation where the potential is at its maximum and the adhesive force (pressure) is zero and z is the separation distance between two planes.

162

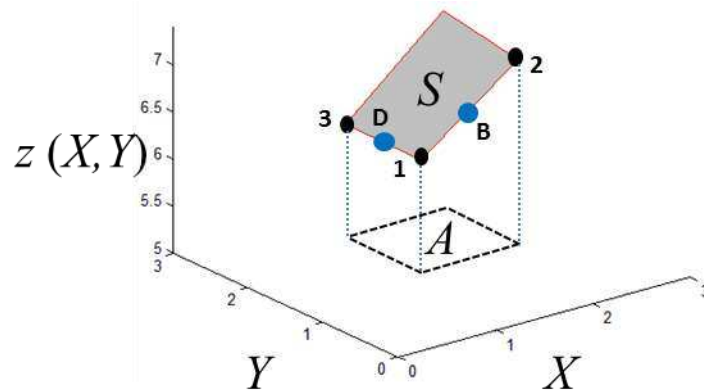
163 Equation 5 is valid for the case of two parallel planes with a separation distance z . In order to
164 be able to use the above formulation in a discretised boundary element formulation, there is a
165 need to approximate the adhesive pressure over the area around a computational node. This is
166 not a straightforward task and a proposed way to approach this is presented in the following
167 paragraph.

168 To facilitate the approximation of the adhesive pressures, it is necessary to consider the
169 configuration of the computational nodes in BEM. Figure 1 represents the cross section of the
170 roughness profile only in one dimension. The real surface topography is a 2-dimensional
171 matrix with every element representing the surface height of a computational node. Figure 2
172 shows a discretised surface with point 1 being the point that surface tensions are being
173 calculated with respect to Equation 5. Substituting the separation value (z) of the node 1 in
174 Equation 5 results in a value of pressure (two black squares in Figure 2) which is not
175 representative of the pressure in the computational domain for point 1 (dashed square around
176 point 1). The dashed square in Figure 2 represents the BEM domain for one computational
177 node at which the pressure is assumed to be constant. Points A, B, C and D (shown by blue
178 dots) are the points of interest at which the separation will largely affect the tensile pressure at
179 point 1. A significant amount of information is missed (if only the pressure at point 1 is taken
180 into account) at the edges of the computational node (points A, B, C and D) due to the shape
181 of the Lennard-Jones potential. Figure 2 shows how separation values at points A, B, C and D
182 affect the integral value of tensile stress over the line integrals moving in X and Y directions.



183

184 Figure 2 Discretisation of the surface in BEM. Point 1 represents the computational node that
 185 adhesion pressure is going to be calculated at.



186

187 Figure 3 Representation of surface separation and its projection on the XY plane. Points
 188 shown are the same as the ones on Figure 2.

189 This problem is valid for movements in both X and Y directions on the surface. In order to
 190 overcome this issue, an approximation is needed to integrate the profile of the Lennard-Jones
 191 potential in both X and Y directions and calculate the two-dimensional average of the pressure.

192 The Lennard-Jones pressure formulation of Equation 5 is dependant only on the separation of
 193 surfaces in normal direction and the integration should be carried out in X and Y directions as
 194 a surface integral. Therefore the following formulation is proposed:

$$195 \quad p(i) = \frac{1}{a^2} \iint p(z) ds \quad (7)$$

196 where a is the length of the computational elements in X and Y direction, and ds is the
 197 differential of the surface representing the surface heights. For the BEM calculations, the
 198 surface integral needs to be carried out with respect to X and Y with the following integration:

$$199 \quad p(i) = \frac{1}{a^2} \iint \left\{ f(X, Y, z(X, Y)) \sqrt{\left(\frac{\partial z}{\partial X}\right)^2 + \left(\frac{\partial z}{\partial Y}\right)^2 + 1} \right\} dA \quad (8)$$

200 Where f is a function that we need to integrate on the surface (in this case, the adhesive pressure
 201 function), $z(X, Y)$ is the separation function with respect to X and Y coordinates and dA is the
 202 differential of the projection area on the XY plane as shown in Figure 3. Equation 8 considers
 203 the changes in the mean value of the adhesive pressure function by the increment of surface
 204 area due to roughness. It should be noted that shape of the surface nodes (in terms of their
 205 sharpness, etc) affect the intensity of the average separation and therefore the average adhesive
 206 pressure. We are only able to integrate the separations from point 1 to point 2 in X direction
 207 and from point 1 to point 3 in Y direction. Ideally, we should integrate from point A to point B
 208 in X and point C to point D in Y direction. This is impossible since we do not have information
 209 regarding the heights for point A, B, C and D.

210 Ideally, having a surface integral on the area A would enable the calculation of the pressure.
 211 That needs the equation of z as a function of X and Y to be determined. This is possible using
 212 bilinear interpolation technique. However, this will give a non-linear function of z based on X
 213 and Y and integrating Equation 8 will be impossible analytically. Instead by substituting
 214 Equation 5 into Equation 8 and writing $dA = dXdY$, and knowing that $dX = \frac{dX}{dz} dz$ and $dY =$
 215 $\frac{dY}{dz} dz$ the integration can take the form:

$$216 \quad p(i) = \frac{1}{a^2} \int_{Y_1}^{Y_3} \int_{X_1}^{X_2} \left\{ \frac{8w_0}{3z_0} \left\{ \left(\frac{z_0}{z}\right)^9 - \left(\frac{z_0}{z}\right)^3 \right\} \sqrt{\left(\frac{\partial z}{\partial X}\right)^2 + \left(\frac{\partial z}{\partial Y}\right)^2 + 1} \right\} \left(\frac{dX}{dz} dz\right) \left(\frac{dY}{dz} dz\right) \quad (9)$$

217 in which X and Y stand for the position of points in the X and Y direction and the subscripts
 218 represent the nodes of interest. Solving the integral of Equation 9 results in the adhesive
 219 pressure formula for each node to be calculated by:

$$\begin{aligned}
 220 \quad p(i) &= \left(\frac{1}{a^2} \left(\sqrt{\left(\frac{z_2 - z_1}{X_2 - X_1} \right)^2 + \left(\frac{z_3 - z_1}{Y_3 - Y_1} \right)^2} + 1 \right) \left(\frac{X_2 - X_1}{z_2 - z_1} \right) \left(\frac{Y_3 - Y_1}{z_3 - z_1} \right) \right) \int_{z_1}^{z_3} \int_{z_1}^{z_2} \left\{ \frac{8w_0}{3z_0} \left(\frac{z_0}{z} \right)^9 \right. \\
 221 \quad &\quad \left. - \left(\frac{z_0}{z} \right)^3 \right\} dz dz \quad (10)
 \end{aligned}$$

222 Knowing that $X_2 - X_1 = Y_2 - Y_1 = a$ and solving the double integration, the final equation is
 223 solved as:

$$\begin{aligned}
 224 \quad p(i) &= \left(\left(\sqrt{\left(\frac{z_2 - z_1}{X_2 - X_1} \right)^2 + \left(\frac{z_3 - z_1}{Y_3 - Y_1} \right)^2} + 1 \right) \left(\frac{1}{z_2 - z_1} \right) \frac{w_0}{3z_0} \right) \left(\frac{4z_0^3}{z_2^2} - \frac{z_0^9}{z_2^8} + \frac{z_0^9}{z_1^8} \right. \\
 225 \quad &\quad \left. - \frac{4z_0^3}{z_1^2} \right) \quad (11)
 \end{aligned}$$

226 In order to solve the adhesive problem using Equation 11, information from the adjacent nodes
 227 in X and Y direction (2 and 3) is needed. Therefore the BEM algorithm should start calculating
 228 the adhesive pressures from one row (in either X and Y direction) and complete the pressure
 229 profile by moving across the columns one by one. It can be noted that Equation 9 can be used
 230 when H or z is represented as a function of X and Y e.g. for the case of parabolic or spherical
 231 smooth contacts and an analytical model of adhesive pressures can be developed. This will be
 232 the subject of future investigations and is not within the scope of the present paper.

233 **2.3 Numerical approach**

234 The non-adhesive contact model explained in Section 2.1 should now be modified to account
 235 for the adhesive pressures calculated at separated computational nodes using Equation 11. This
 236 needs a careful definition of surface separations between all computational nodes since
 237 separation g defined after Equation 3 has to now accommodate atomic separation z in Equation
 238 11. Due to the shape of Lennard-Jones potentials, separation less than z_0 will result in high
 239 compressive pressures. Since compressive pressures are already calculated using the non-
 240 adhesive algorithm of Section 2.1, positive pressures should be truncated out of adhesive
 241 calculations. In order to overcome this, a relationship between atomic separation (z) and
 242 continuum separation (g) is used as the following (12):

243
$$g + z_0 = z \quad (12)$$

244 This new separation (z) will be used in Equation 11 to calculate the adhesive pressures.
 245 Although this will shift the profile of Lennard-Jones for z_0 to the left, Medina and Dini (12)
 246 showed this can be tolerated due to the sharp slope of the shape of the pressure profile. The
 247 non-adhesive formulation of Equation 3 is now converted to an adhesive problem as the
 248 following:

$$p_i > 0 \quad g_i = 0$$

$$p_i < 0 \text{ based on Equation 11} \quad g_i > 0$$

$$W = \iint p(X, Y) dXdY$$

249 This new set of equations needs to be solved in an iterative process. Previously, for a non-
 250 adhesive contact, pressures less than zero could be simply truncated out of simulation by
 251 replacing them with zero pressures. For adhesive contact, the negative pressures will be present
 252 and they disturb the gap and elastic deformation balance. Solving the new contact problem with
 253 adhesion needs a robust numerical algorithm since introduction of negative (adhesive)
 254 pressures can easily lead to difficulty in convergence. A new numerical algorithm is presented
 255 here that was shown to work for all contact cases including low and large Tabor parameters for
 256 both smooth and rough surfaces. The detailed description of the algorithm is given below:

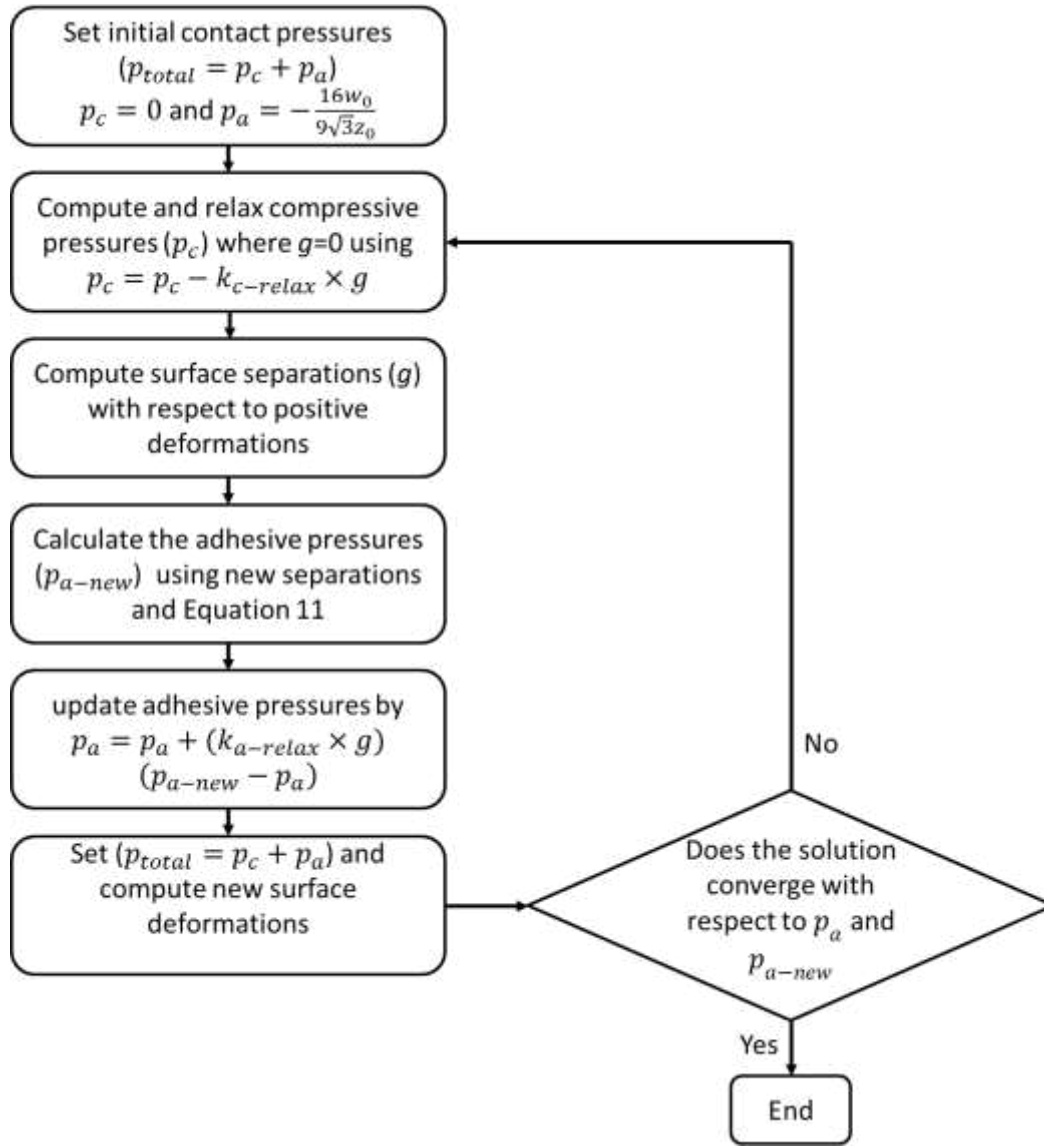
- 257 • An initial contact pressure distribution is assumed on the entire surface which is a
 258 combination of the positive (p_c - compressive) and the negative (p_a - adhesive)
 259 pressures. $p_{total} = p_c + p_a$. Selection of a suitable initial adhesive pressure is critical
 260 in our algorithm and defines how quick the final solution is converged. It was shown
 261 that a constant negative pressure of $p_a = -\frac{16w_0}{9\sqrt{3}z_0}$ will result in the quickest and most
 262 efficient computation for unloading of contact. For loading (jumping into contact) we
 263 start from zero adhesion.
- 264 • Calculate the positive pressures using Equation 3 and replacing negative pressures by
 265 zero. The total pressure p_{total} is used to calculate the surface deformations in this stage.
 266 The relaxation in this stage updates the positive pressures with the following process:
 267 $p_c = p_c - k_{c-relax} \times g$ where $k_{c-relax}$ is the relaxation factor for positive pressures
 268 and g is the separation at each node. Values in the range of 0.00000001 and 0.01 were

269 used depending on the elastic properties of surfaces. This relaxation factor was
270 optimised independently only for positive pressures.

- 271 • The separation at points of zero pressures were calculated and adhesive pressures
272 (p_{a-new}) were calculated at every node using Equation 11.
- 273 • The residuals of surface points were calculated in a new iteration loop where only
274 adhesive pressures p_a were relaxed using a new relaxation coefficient as the following:
275 $p_a = p_a + (k_{a-relax} \times g) \times (p_{a-new} - p_a)$ where $k_{a-relax}$ is the relaxation factor for
276 adhesive pressures and is independent of $k_{a-relax}$. This coefficient is in the range of
277 0.0000001 and 0.1 and dependant on the local Tabor parameter. Here we used the
278 inverse root-mean-square curvature which can be interpreted as the local radius of
279 curvature to identify the local Tabor parameter in the presence of roughness. The
280 residuals and surface deformations were calculated by the total pressure p_{total} being
281 updated as $p_{total} = p_c + p_a$ and new surface deformations were calculated.
- 282 • This process was undertaken until a convergence was achieved between p_a and p_{a-new} .
283 It should be noted that relaxation of positive and negative pressure was carried out
284 independently in two interconnected loops. The loop for the positive pressure
285 calculations was done prior to calculation of negative pressures and was carried out in
286 every adhesive pressure loop.

287 The convergence criteria in this model was set as the average of the residuals for positive
288 pressures to be less than $z_0 \times 10^{-6}$.

289 A schematic of the algorithm is represented in Figure 4.



290

291

Figure 4 Schematics of the numerical algorithm

292 3 Results

293 3.1 Simulation of smooth surfaces

294 For the sake of model validation, the case of smooth spheres with a range of Tabor parameters

295 has been studied and the results of dimensionless load $\left(\frac{W}{2\pi R^* w_0}\right)$ versus dimensionless approach

296 $\left(\frac{\alpha}{z_0}\right)$ were compared to the existing theories. It is tricky to capture the adhesive contact

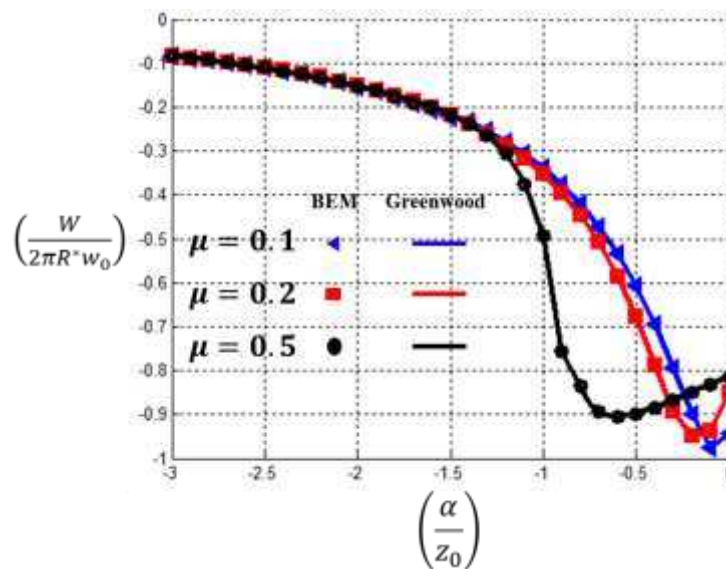
297 behaviour of surfaces for Tabor parameters ranging from $0.1 < \mu < 3$ since they are describing

298 the transition from DMT to JKR theories. In this case, a comparison with the model of

299 Greenwood (8) is represented. The Tabor parameter is defined as $\mu = \frac{R^* \frac{1}{3} w_0^{\frac{2}{3}}}{E^* \frac{2}{3} z_0}$ where R^* is the

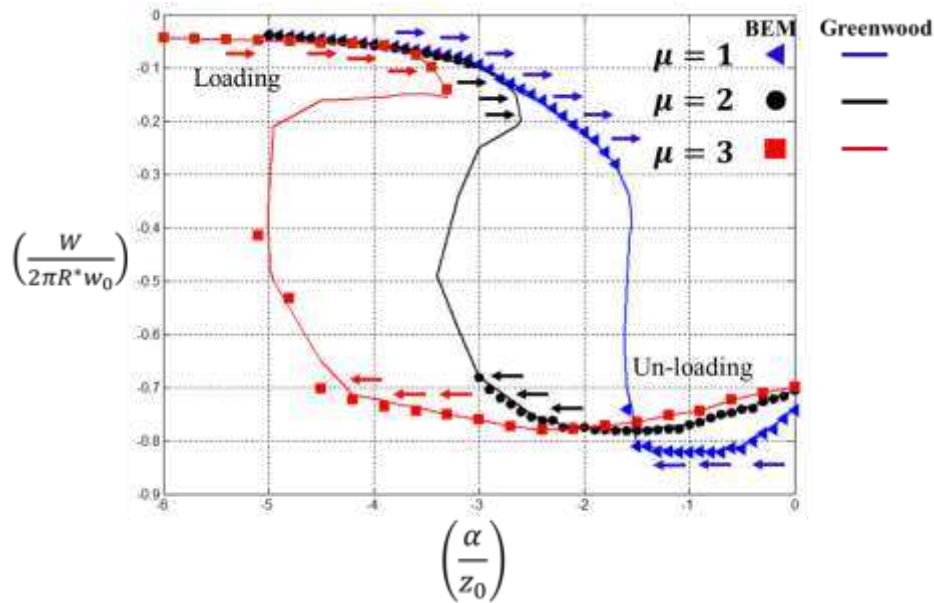
300 equivalent radius of curvature and for the case of sphere on flat surface is the radius of the

301 curvature of the sphere. Figure 5 shows the comparison of our model with model of Greenwood
 302 at values of $\mu = 0.1, 0.2$ & 0.3 and Figure 6 shows the comparison for $\mu = 1, 2$ & 3 where a
 303 good agreement is observed. The simulations can capture the adhesive pressures for negative
 304 values of separation. For the case of higher Tabor parameters (Figure 6), Greenwood has
 305 shown an S-shape behaviour in the loading-unloading curve. This phenomena can be captured
 306 by the current numerical model if two different simulations (loading and unloading) are
 307 conducted. However, the simulation cannot capture some part of the adhesive pressure between
 308 loading and unloading. This is due to the nature of this numerical models that need a certain
 309 value of separation as input to the model (displacement controlled) and the model cannot give
 310 two values of pressure for the same separation (inevitable in S-shape profile). This would
 311 become possible by a force-controlled numerical approach. Greenwood has used a solution by
 312 fixing the displacement at the centre of the contact. The arrows on the load-separation curve in
 313 Figure 6 show if the data have been obtained in loading or unloading cycles. It should be noted
 314 that convergence time increased as the Tabor parameter increased and it is due to higher
 315 adhesive pressures and higher disturbance of the deformations of positive pressures (non-
 316 adhesive case). An example of the contour of contact pressure as well as cross section of the
 317 total pressure in the middle plain is reported in Figure 7.



318

319 Figure 5 Comparison between the current model and Greenwood's model for small values of
 320 Tabor parameters. Dimensionless load is plotted against dimensionless approach.



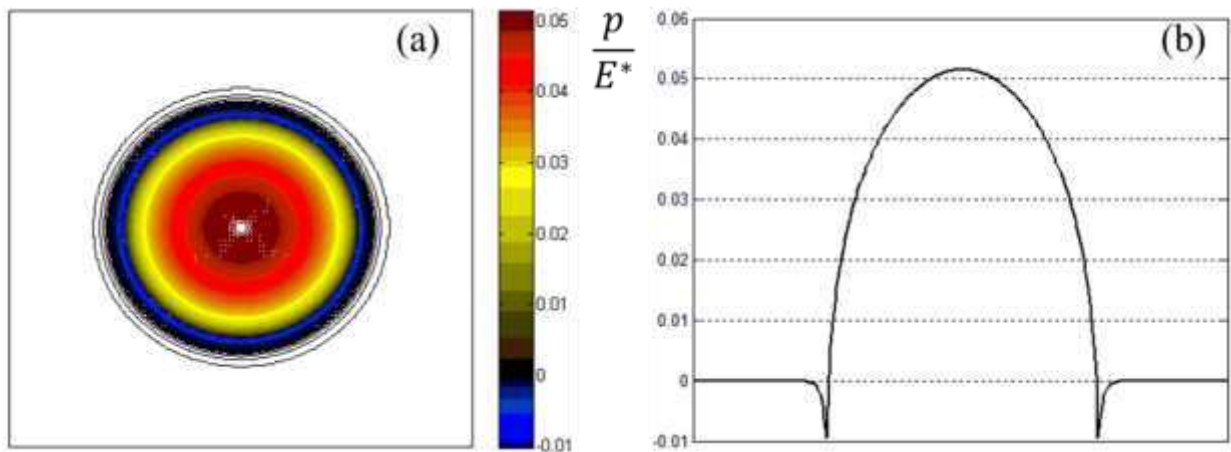
321

322

323

Figure 6 Comparison between the BEM model and the Greenwood model for Tabor parameters of $\mu=1, 2$ and 3 . Dimensionless load is plotted against dimensionless approach.

324



325

326

327

Figure 7 Representation of the (a) contour of contact pressure and (b) cross section of the pressure profile for the case of smooth plane in contact with a rigid indenter.

328

329 3.2 The contact mechanics challenge

330

331

332

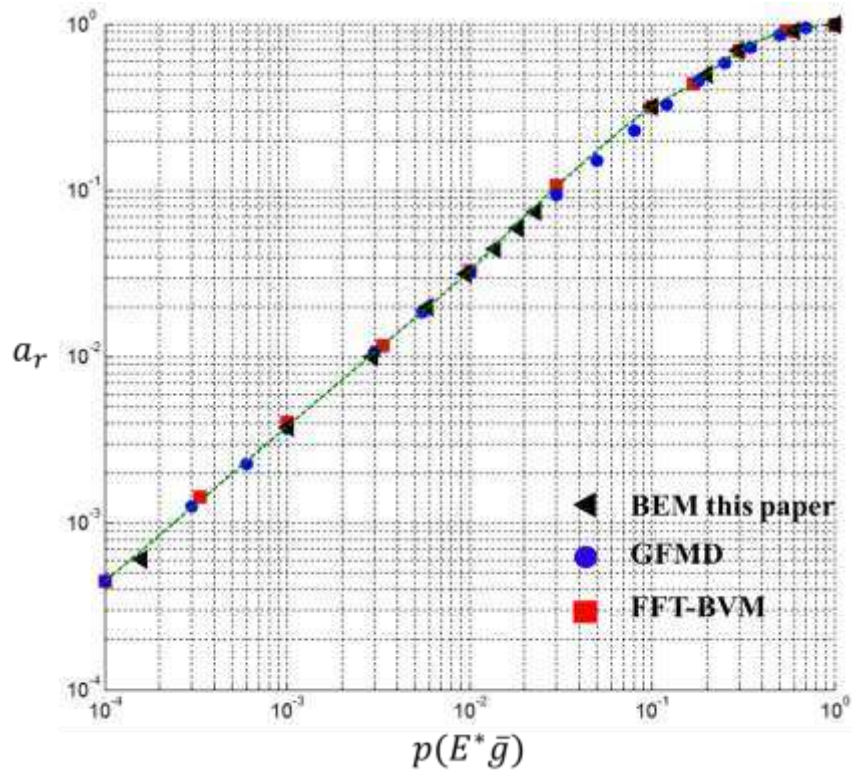
333

334

335

In December 2015, Martin Müser has introduced a contact mechanics challenge where a pre-defined self-affined surface was created and scientists were asked to use their own in-house numerical techniques to calculate the contact between the surface and a rigid flat surface. The results presented in a published paper (11) show a reasonable agreement between numerical results e.g. Green Function Molecular Dynamics (GFMD), All-atom MD, FFT-BVM, etc. The purpose of this section is to use the same surface used in (11) and to reproduce the results with

336 the numerical model presented in this paper for comparison. Initially, the parameters used in
337 the challenge will be summarised here. The surface was normalised to have a root mean square
338 gradient of $\bar{g} = 1$, minimum height of zero and a maximum of $5.642 \mu\text{m}$ and the surface was
339 representing an area of $0.1\text{mm} \times 0.1\text{mm}$. The inverse root mean square of the curvature which
340 can be used as typical local radius of curvature was defined as $R^* = 60\text{nm}$. In addition, the
341 equivalent elastic modulus was set as $E^* = 25 \text{MPa}$, the work of adhesion was set as $w_0 =$
342 $50 \text{mJ}/\text{m}^2$ and the equilibrium separation was $z_0 = 2.071\text{nm}$. The simulations were carried
343 out using the current BEM model and adopting the parameters in the challenge. The results for
344 the relative contact area against normalised pressure and the gap distribution in the middle
345 plane of the contact has been reproduced. Figure 8 shows the comparison of the current model
346 (BEM) with two selected numerical results i.e. GFMD and FFT-BVM from the challenge. The
347 result shows a good quantitative agreement between BEM and the result of the challenge. The
348 x axis represents the average of contact pressure across the whole nominal area normalised by
349 the $E^* \bar{g}$ and the y axis is the ratio of contacting areas with the total nominal area. Figure 9
350 presents the profile of the gap in a cross section in the middle of contact ($x = 50\mu\text{m}$) and
351 compares the results of current model with GFMD simulations presented in (11) and a good
352 agreement is found. The small discrepancy of the results can be due to the differences in the
353 resolution of the simulations. The simulations carried out in this model use a discretisation of
354 4096×4096 .



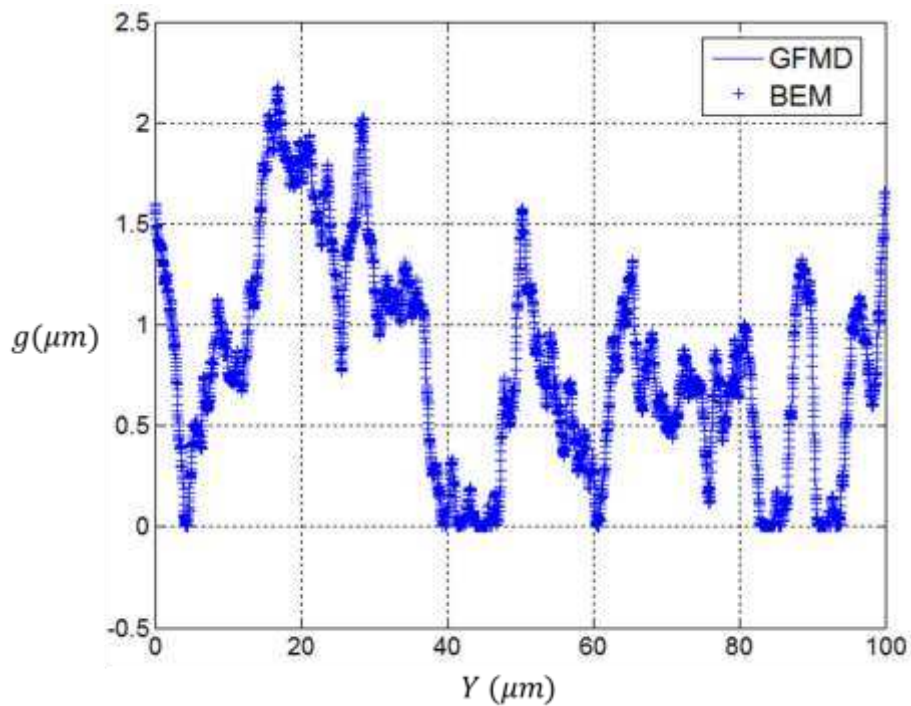
355

356

357

358

Figure 8 The relative contact area (a_r) against normalised average pressure ($p/E^* \bar{g}$) and the comparison with the contact mechanics challenge (11). GFMD and FFT-BVM have been chosen for comparison.



359

360

361

362

Figure 9 Gap distribution of deformed surfaces (g) at a cross section in the middle of contact ($X=50 \mu\text{m}$ in the contact mechanics challenge problem definition). The results of BEM in this work are compared with the GFMD results from (11).

363 3.3 Effect of roughness

364 Numerical methods such as the one developed in this paper are ideal for studying the contact
 365 behaviour of deterministic rough surfaces. Here we have generated rough surfaces with self-
 366 affine properties to examine the effect of different surface characteristics on the real area of
 367 contact and stickiness of surfaces. The pull-off force (force needed to completely separate the
 368 surfaces) and the contact area ratio were also plotted for different surfaces at different Tabor
 369 parameters. Surfaces are generated using the Power Spectrum Density (PSD) as reported by
 370 Persson (27). Random numbers were used along with Fourier transforms of the height function
 371 ($\tilde{h}(q)$). The height spectrum $C(q)$ was defined as:

$$372 \quad C(q) = C(q_r) \times \begin{cases} 1 & \lambda_r < \frac{2\pi}{q} \leq L \\ (q/q_r)^{-2(1+H)} & \lambda_s \leq \frac{2\pi}{q} < \lambda_r \\ 0 & \end{cases} \quad (13)$$

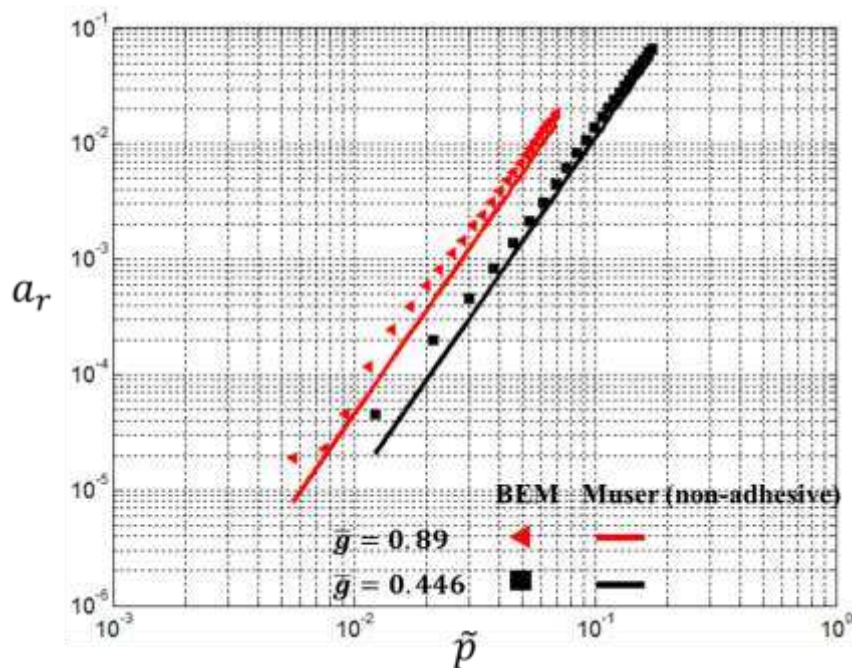
373 In which λ_r is the roll-off wavelength, λ_s is the short wavelength cut-off, L is the length of the
 374 surface in each dimension, $q_r = \frac{2\pi}{\lambda_r}$ and H is the Hurst parameter which is calculated by $H =$
 375 $3 - D_f$ where D_f is the fractal dimension. All the surfaces generated with this method have a
 376 mean of zero.

377 Müser (28) has shown that the formula for relative contact area firstly introduced by Pastewka
 378 and Robbins (29) can accurately capture the non-adhesive contact behaviour of rough surfaces
 379 and introduced a new formula by improving the Pastewka and Robbins criteria using a new
 380 equation for contact area by eliminating the mean-field approximation.

$$381 \quad a_r(k\tilde{p}) = \pi a_0^2 \left(1 - \frac{1}{2k^2\tilde{p}^2} \right) \text{erf}(k\tilde{p}) + \frac{\exp(-k^2\tilde{p}^2)}{\sqrt{\pi}k\tilde{p}} \quad (14)$$

382 In Equation 14, a_r is the relative real contact area, k is a number that is often two for real
 383 engineering surfaces, \tilde{p} is calculated by $\tilde{p} = \frac{3L}{4\sqrt{\pi}E^*\bar{g}a_0^2}$ and is a physical representation of the
 384 average contact pressures; L is the total applied load on the nominal area, \bar{g} is the root mean
 385 square gradient of surface roughness and a_0 is the radius of the nominal contact area. Equation
 386 14 is used in this work to analytically predict the contact area in the case of adhesion-less
 387 contact and the BEM is used to predict the contact area for adhesive contact. The aim of this
 388 section is then to see the effect of adhesion on the real contact area for rough surfaces. Figure
 389 10 shows the comparison between the adhesive model ($\mu = 3$) presented in this paper and the
 390 non-adhesive theory of Müser (28). The discrepancy of adhesive and non-adhesive contacts is

391 more significant for higher values of the Tabor parameter. Results clearly show that adhesion
 392 is playing an important role in increasing the relative contact area as expected. The other point
 393 to highlight is that the model -with a very good quantitative agreement- can follow the trend of
 394 area of contact in the presence and absence of adhesion. This interesting numerical finding is
 395 valid for both values of root mean square gradient of surface roughness. This means that for
 396 cases with larger radius and softer materials the real contact area is significantly affected by
 397 adhesion. Physical problems such as contact and friction of rubbers, contact of biomaterials,
 398 cartilages and cells and contact of viscoelastic solids can be largely dependent on adhesion.
 399 Ignoring surface roughness and adhesion in such areas will considerably misrepresent the
 400 contact mechanics and evaluation of the corresponding friction and wear. For instance, for
 401 small values of average pressure (\bar{p}), real area for the case of adhesive contact is larger than
 402 the area of non-adhesive contact by a factor of 2 or 3. This is a large underestimation of the
 403 contact area which can eventually under-predict friction and wear by the same factor. This
 404 highlights the importance of models such as the one developed in this work to deterministically
 405 calculate real contact area and pressure distribution in the presence of adhesion.



406

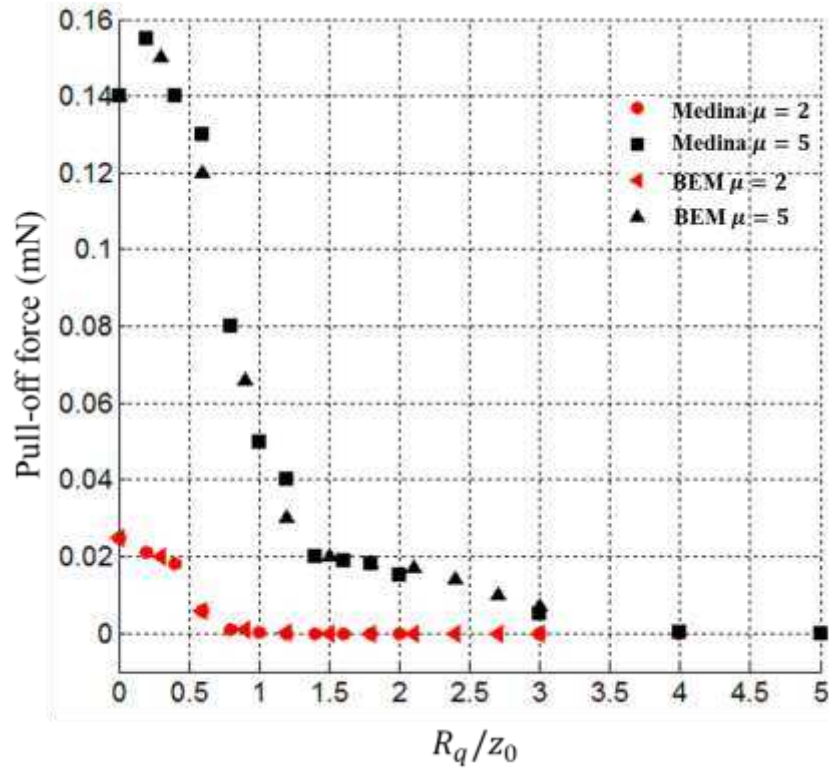
407 Figure 10 Comparison between the theory of Muser (28) for non-adhesive contact of rough
 408 surfaces and the BEM for adhesive contacts. Relative contact area is plotted against pressure
 409 (\bar{p}) for two values of \bar{g} .

410 3.3.1 Effect of roughness on the pull-off force

411 In the adhesive contact of surfaces, when the approach of the bodies is negative, adhesive forces
 412 will deform the surfaces and there may be body interference between solid surfaces which in

413 turn, causes compressive pressures. The area in which the compressive pressures still exists, is
414 the contact area. The minimum negative force in the process of separating the surfaces is called
415 the pull-off force. This is the minimum negative force required to completely separate the
416 surfaces. In this section, the effect of surface roughness and the Tabor parameter on the pull-
417 off force calculated by BEM is presented. The results are then compared with the numerical
418 results produced by Medina and Dini (12) to see how results from a more complete surface
419 integral method will differ from a line integral approach. The simulation parameters are set as
420 $(R^* = 100\mu m, E^* = 50GPa, z_0 = 0.3nm, w_0 = 0.29 \frac{J}{m^2} \text{ and } w_0 = 0.075 \frac{J}{m^2})$ in order to get
421 Tabor parameters 5 and 2 respectively and the results are plotted in Figure 11.

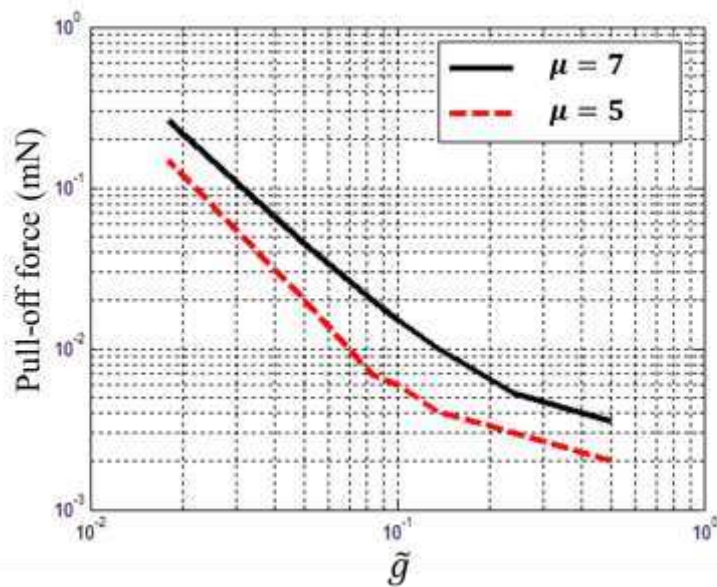
422 It should be noted that the main part of the results section of this paper looks at validation of
423 the new mathematical model and the algorithm proposed, with the existing theories in the
424 literature for both smooth and rough surfaces. This is to show how effectively Lennard-Jones
425 potentials could be applied on a rough surface in BEM to predict adhesion in contact
426 mechanics. In order to further study the effect of roughness parameters on adhesion, we have
427 extended our study to investigate the effect of RMS slope \bar{g} on the adhesion. Simulations are
428 carried out with the same root mean square roughness (R_q) of $2z_0$ but different \bar{g} values and
429 the effect of \bar{g} on the pull-off force was investigated.



430

431
432

Figure 11 Effect of R_q on the pull-off force for randomly rough surfaces and the comparison with the results of Medina and Dini (12)



433

434
435

Figure 12 Effect of root mean square gradient of surface roughness on the magnitude of pull-off force for the case of $\mu = 5$ and $\mu = 7$, $R_q = 2z_0$

436

437
438

Figure 12 represents the results when the root mean square roughness of the surface is constant and only the mean square gradient of roughness (\tilde{g}) is altered to see the effect on the force needed to separate surfaces. The results clearly show that increasing the \tilde{g} will result in

439 decreasing the pull-off force and this is independent of the R_q value of the surface roughness.
440 The value of \bar{g} represent how sharp or blunt the surface asperities (at least at the resolution that
441 topography is defined) are which in turn affects the separation of surfaces near the edge of
442 contact.

443 The simulations presented in this paper study the effect of surface topography on the adhesive
444 pressures in the contact of nominally flat surfaces. The effect of adhesion is shown to be
445 important in determination of real contact area. Results of Figure 10 show the difference of the
446 relative contact area in the case of adhesive contact with the case of non-adhesive contact
447 reported by Müser. It also proves the fact that adhesion increases the real area of contact as
448 expected. It was shown previously that increasing the root mean square of surface roughness
449 will reduce the effect of adhesive pressures on the surfaces in contact. This is due to higher
450 separation of surface points. In addition, rougher surfaces will experience higher compressive
451 pressures at the point of higher topography peaks and the small adhesive pressures will be
452 negligible compared to the compressive ones. The pull-off force needed to separate surfaces
453 generally decreases as the root mean square roughness increases.

454 It should be highlighted that we have investigated the effect of these parameters (R_q and \bar{g})
455 and have numerically shown the importance of both. The recent theoretical works of Ciavarella
456 (2, 30, 31) have highlighted alternative surface and material parameters responsible for the area
457 of contact and discussion around stickiness criteria was made. They used different independent
458 theories (BAM, Persson-Tosatti (10)) along with DMT theories previously reported by Persson
459 and Scaraggi (32). He has shown that macroscopic features of surface roughness such as R_q
460 and the low wavevector cut-off of surface roughness and the ratio of work of adhesion and the
461 equivalent Young's modulus are important parameters for stickiness. This is interesting and
462 we believe our results do not contradict with the criteria of Ciavarella. We have therefore
463 carried out an investigation to include the effect of both RMS and RMS slope in the adhesive
464 force calculations of rough surfaces. Recently, Li et al. (22) have demonstrated the effect of
465 the Johnson parameter (33) in the adhesive contact of wavy surfaces. They have introduced a
466 modified version of the Johnson parameter that considers the fractal properties of rough
467 surfaces and argued that the adhesion between rough surfaces is dependent on this new
468 parameter for larger values of Tabor parameter (JKR-limit). The modified version of the
469 Johnson parameter (α^*) was formulated as:

$$470 \quad \alpha^* = \left(\frac{4w_0 q_1^{0.8H-1}}{\pi E^* h^2 q_0^{0.8H}} \right)^2 \quad (15)$$

471 in which H is the Hurst exponent of the fractal surface, h is the RMS roughness, q_0 and q_1 are
 472 the smallest and largest wavevectors respectively. We have plotted the pull-off force with
 473 respect to the modified Johnson parameter (α^*) for three values of Tabor parameter ($\mu =$
 474 2, 5 and 7) and results are presented in Figure 13. Results indicate that normalising our pull-
 475 off force calculations with respect to the modified Johnson parameter results in very similar
 476 values of the pull-off force. It should be noted that Persson and Scaraggi (32) and Ciavarella
 477 (19) have shown that the pull-off force is almost independent of the large wavevector
 478 component. Our results show that this new modified dimensionless parameter that includes
 479 both RMS and RMS slope, small and large wavevectors could be a reasonable but not fully
 480 comprehensive stickiness criteria for the adhesion of rough surfaces with fractal properties in
 481 JKR limit. This is because our results show small discrepancies at different Tabor parameters
 482 (JKR-limit) which suggests that the parameter could somehow be modified. Our simulation
 483 data are also in-line with the results of Li et al.(22) which showed the same dependency.

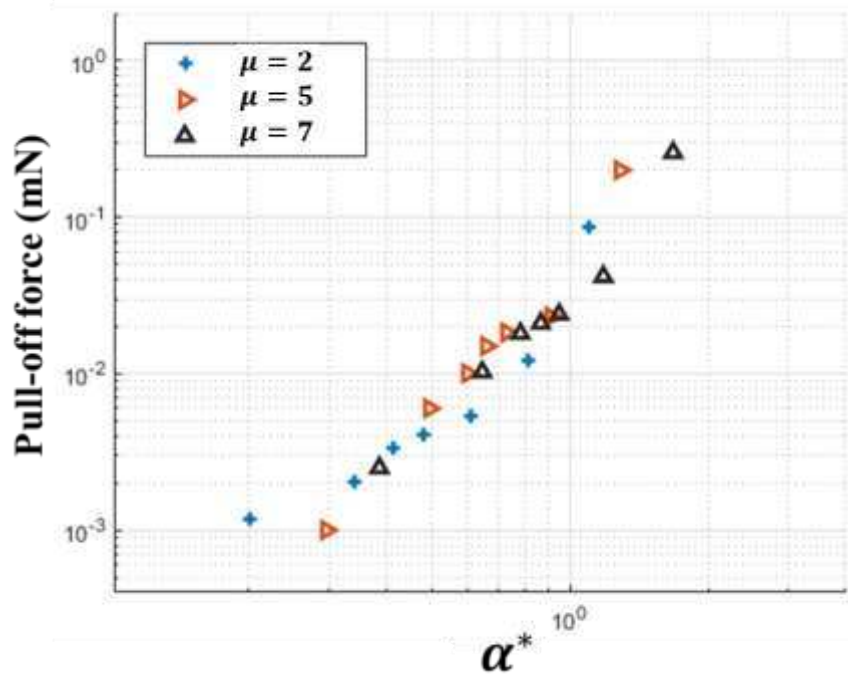
484 In order to test the numerical model with other stickiness criteria, we have used the theory of
 485 Ciavarella (30) which was based on the BAM model. In his model, Ciavarella introduced new
 486 adhesion criteria along with those of Persson and Tosatti (10) and has shown that both models
 487 although from completely different origins, predict very similar stickiness criteria. The
 488 stickiness criteria of Ciavarella was reported as the following:

$$489 \quad R_q < \sqrt{\beta \lambda_L I_a} \quad (16)$$

490 in which β is 0.6 in his theory, λ_L is the large wavelength of the surface roughness and I_a is
 491 (w_0/E^*). This criteria suggests that only RMS roughness and the large wavelength of
 492 roughness (small wavevector) are responsible for stickiness. In order to compare our results
 493 with this theory, we have plotted our pull-off force calculations against $\left(\frac{R_q^2 E^*}{\lambda_L w_0} \right)$ for different
 494 cases at Tabor parameters of $\mu = 2, 5$ and 7 and the results are plotted in Figure 14. It is
 495 interesting to see that the new parameter is a good stickiness criteria for this range of Tabor
 496 parameter since the results of pull-off force against this stickiness parameter matches almost
 497 perfectly for all three values of Tabor parameter. This suggests that Equation 16 (Ciavarella's

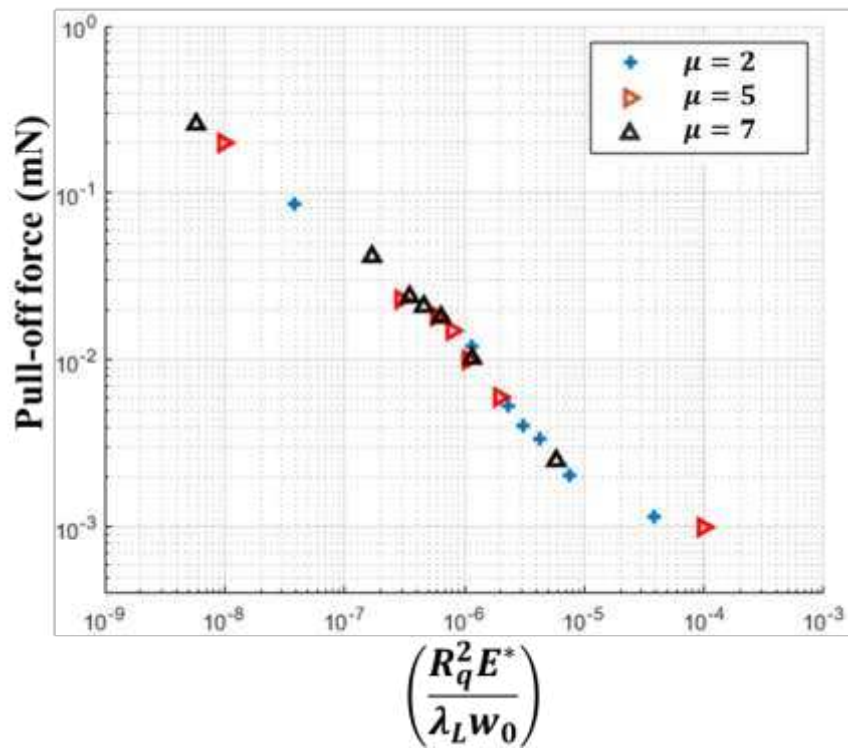
498 stickiness model) is the most accurate and reasonable stickiness criteria based on our
499 simulations.

500 We believe our model, could be a platform for the future development of adhesion models for
501 real rough surfaces and more robust stickiness criteria for a wider range of materials could be
502 achieved.



503

504 Figure 13 The effect of the modified Johnson parameter on the pull-off force for three values
505 of Tabor parameter ($\mu = 2, 5$ and 7)



506

507 Figure 14 Pull-off force against the stickiness criteria of Ciavarella (30) for $\mu = 2, 5$ and 7

508 4 Conclusions

509 This paper presents the development of a BEM model for contact mechanics of rough surfaces.
 510 Adhesion is considered by means of inter-atomic Lennard-Jones potential and a new surface
 511 integration approach is incorporated. The model extends the model of Medina and Dini where
 512 a line integration of the Lennard-Jones potential was developed. The model shows very good
 513 quantitative agreement with the model of Greenwood for medium range Tabor parameter and
 514 reproduces exact solutions of the contact mechanics challenge introduced by Müser. The
 515 deterministic nature of the model enables us to analyse the adhesive contact of surfaces with
 516 any complex geometry and investigate the local pressures and deformations at micron and
 517 nano-scales. Therefore the effect of roughness on the adhesion is studied with a focus on the
 518 root mean square gradient of roughness and the following conclusions are drawn:

- 519 • A new mathematical equation is developed in this work to evaluate adhesion of rough
 520 surfaces and can be used in BEM simulations. The incorporation of the mathematical
 521 equation is simple and the algorithm used in this work is very efficient.
- 522 • It was numerically shown that inclusion of adhesion in the deterministic contact
 523 calculations of rough surfaces affects the real contact area ratio. This was shown by
 524 comparing the numerical results of BEM developed in this paper by analytical model

525 developed by Müser. It was revealed that the root mean square gradient of roughness
526 not only affect the real area of contact in the non-adhesive case, but also affects the area
527 of contact in the case of adhesive contact.

- 528 • We have presented that not only the R_q value can significantly reduce the adhesion
529 effect, but also the root mean square gradient of surface roughness can significantly
530 affect the adhesive forces. Higher root mean square gradient results in lower adhesive
531 force and lower pull-off force needed to separate surfaces. This is believed to be due to
532 the difference in the real area of contact cause by the shape of asperities.
- 533 • We have investigated the effect of the modified Johnson parameters (that include both
534 fractal properties and RMS) on the stickiness of rough surfaces and have shown that
535 this dimensionless parameter could be a reasonable but not fully comprehensive
536 stickiness criteria for the contact of rough surfaces.
- 537 • Furthermore, we have shown that the criteria introduced by Ciavarella almost perfectly
538 matches our simulation results and by far is the best stickiness criteria based on our
539 simulations.

540 **Acknowledgement**

541 The authors are grateful to Dr Mark Wilson from University of Leeds for kindly sharing his
542 thoughts on the mathematical rigor of the developed model. Authors are also thankful to
543 Professor Martin Müser from Saarland University for kindly sharing the raw data reported in
544 the contact mechanics challenge paper. This work is supported by the Engineering and Physical
545 Sciences Research Council (Grant Number EP/001766/1) as a part of 'Friction: The Tribology
546 Enigma' Programme Grant ([www. friction.org.uk](http://www.friction.org.uk)), a collaboration between the Universities of
547 Leeds and Sheffield.

548

549

550

551

552

553

554

555

556

557

558

559

560

561

562

563

564 **References**

- 565 1. Israelachvili JN. Intermolecular and surface forces: Academic press; 2015.
- 566 2. Ciavarella M, Joe J, Papangelo A, Barber J. The role of adhesion in contact mechanics.
567 Journal of the Royal Society Interface. 2019;16(151):20180738.
- 568 3. Johnson KL, Kendall K, Roberts A. Surface energy and the contact of elastic solids.
569 Proc R Soc Lond A. 1971;324(1558):301-13.
- 570 4. Derjaguin BV, Muller VM, Toporov YP. Effect of contact deformations on the
571 adhesion of particles. Journal of Colloid and interface science. 1975;53(2):314-26.
- 572 5. Tabor D. Surface forces and surface interactions. Plenary and Invited Lectures:
573 Elsevier; 1977. p. 3-14.
- 574 6. Maugis D. Adhesion of spheres: the JKR-DMT transition using a Dugdale model.
575 Journal of colloid and interface science. 1992;150(1):243-69.
- 576 7. Muller V, Yushchenko V, Derjaguin B. On the influence of molecular forces on the
577 deformation of an elastic sphere and its sticking to a rigid plane. Journal of Colloid and
578 Interface Science. 1980;77(1):91-101.
- 579 8. Greenwood J. Adhesion of elastic spheres. Proceedings of the Royal Society of London
580 Series A: Mathematical, Physical and Engineering Sciences. 1997;453(1961):1277-97.
- 581 9. Fuller K, Tabor D. The effect of surface roughness on the adhesion of elastic solids.
582 Proceedings of the Royal Society of London A Mathematical and Physical Sciences.
583 1975;345(1642):327-42.
- 584 10. Persson B, Tosatti E. The effect of surface roughness on the adhesion of elastic solids.
585 The Journal of Chemical Physics. 2001;115(12):5597-610.
- 586 11. Müser MH, Dapp WB, Bugnicourt R, Sainsot P, Lesaffre N, Lubrecht TA, et al.
587 Meeting the contact-mechanics challenge. Tribology Letters. 2017;65(4):118.
- 588 12. Medina S, Dini D. A numerical model for the deterministic analysis of adhesive rough
589 contacts down to the nano-scale. International Journal of Solids and Structures.
590 2014;51(14):2620-32.

- 591 13. Solhjo S, Vakis AI. Continuum mechanics at the atomic scale: Insights into non-
592 adhesive contacts using molecular dynamics simulations. *Journal of Applied Physics*.
593 2016;120(21):215102.
- 594 14. Wriggers P, Zavarise G. Computational contact mechanics. *Encyclopedia of*
595 *computational mechanics*. 2004.
- 596 15. Rey V, Ancaix G, Molinari J-F. Normal adhesive contact on rough surfaces: efficient
597 algorithm for FFT-based BEM resolution. *Computational Mechanics*. 2017;60(1):69-81.
- 598 16. Pastewka L, Robbins MO. Contact between rough surfaces and a criterion for
599 macroscopic adhesion. *Proceedings of the National Academy of Sciences*. 2014:201320846.
- 600 17. Afferrante L, Ciavarella M, Demelio G. Adhesive contact of the Weierstrass profile.
601 *Proceedings of the Royal Society A: Mathematical, Physical and Engineering Sciences*.
602 2015;471(2182):20150248.
- 603 18. Ciavarella M. Adhesive rough contacts near complete contact. *International Journal of*
604 *Mechanical Sciences*. 2015;104:104-11.
- 605 19. Ciavarella M. A very simple estimate of adhesion of hard solids with rough surfaces
606 based on a bearing area model. *Meccanica*. 2018;53(1-2):241-50.
- 607 20. Pohrt R, Popov VL. Adhesive contact simulation of elastic solids using local mesh-
608 dependent detachment criterion in boundary elements method. *Facta Universitatis, Series:*
609 *Mechanical Engineering*. 2015;13(1):3-10.
- 610 21. Popov VL, Pohrt R, Li Q. Strength of adhesive contacts: Influence of contact geometry
611 and material gradients. *Friction*. 2017;5(3):308-25.
- 612 22. Li Q, Pohrt R, Popov VL. Adhesive Strength of Contacts of Rough Spheres. *Frontiers*
613 *in Mechanical Engineering*. 2019;5:7.
- 614 23. Ghanbarzadeh A, Hassanpour A, Neville A. A numerical model for calculation of the
615 restitution coefficient of elastic-perfectly plastic and adhesive bodies with rough surfaces.
616 *Powder Technology*. 2019;345:203-12.
- 617 24. Bazrafshan M, De Rooij M, Valefi M, Schipper D. Numerical method for the adhesive
618 normal contact analysis based on a Dugdale approximation. *Tribology international*.
619 2017;112:117-28.
- 620 25. Bazrafshan M, de Rooij M, Schipper D. On the role of adhesion and roughness in stick-
621 slip transition at the contact of two bodies: A numerical study. *Tribology international*.
622 2018;121:381-8.
- 623 26. Bhushan B, Majumdar A. Elastic-plastic contact model for bifractal surfaces. *Wear*.
624 1992;153(1):53-64.
- 625 27. Persson B. On the fractal dimension of rough surfaces. *Tribology Letters*.
626 2014;54(1):99-106.
- 627 28. Müser MH. On the contact area of nominally flat hertzian contacts. *Tribology Letters*.
628 2016;64(1):14.
- 629 29. Pastewka L, Robbins MO. Contact area of rough spheres: Large scale simulations and
630 simple scaling laws. *Applied Physics Letters*. 2016;108(22):221601.
- 631 30. Ciavarella M. Universal features in “stickiness” criteria for soft adhesion with rough
632 surfaces. *Tribology International*. 2019:106031.
- 633 31. Ciavarella M, Papangelo A. A modified form of Pastewka–Robbins criterion for
634 adhesion. *The Journal of Adhesion*. 2018;94(2):155-65.
- 635 32. Persson BN, Scaraggi M. Theory of adhesion: Role of surface roughness. *The Journal*
636 *of chemical physics*. 2014;141(12):124701.
- 637 33. Johnson K. The adhesion of two elastic bodies with slightly wavy surfaces.
638 *International Journal of Solids and Structures*. 1995;32(3-4):423-30.

640 **Additional Information**

641 *Information on the following should be included wherever relevant.*

642

643 **Ethics**

644 There is no ethical considerations required for this research.

645

646 **Data Accessibility**

647 The data published in this paper including the contact mechanics code can be accessible upon the
648 request form the corresponding author.

649

650 **Authors' Contributions**

651 AG developed the numerical model, ran the simulations, analysed and interpreted the data and
652 drafted the paper, approved the final version and is accountable for the paper. AN analysed and
653 interpreted the data, contributed to the discussion and revision of the article and gave final approval.

654 **Competing Interests**

655 The author(s) declare that they have no competing interests.

656

657 **Funding Statement**

658 This work is supported by the Engineering and Physical Sciences Research Council (Grant Number
659 EP/001766/1) as a part of 'Friction: The Tribology Enigma' Programme Grant ([www. friction.org.uk](http://www.friction.org.uk)), a
660 collaboration between the Universities of Leeds and Sheffield.

661

662 **Acknowledgments**

663 The authors are grateful to Dr Mark Wilson from University of Leeds for kindly sharing his thoughts
664 on the mathematical rigor of the developed model. Authors are also thankful to Professor Martin
665 Müser from Saarland University for kindly sharing the raw data reported in the contact mechanics
666 challenge paper. This work is supported by the Engineering and Physical Sciences Research Council
667 (Grant Number EP/001766/1) as a part of 'Friction: The Tribology Enigma' Programme Grant ([www. friction.org.uk](http://www.friction.org.uk)), a collaboration between the Universities of Leeds and Sheffield.

669 **Disclaimer**

670 N/A

671